

Mixed-metal butterfly acetamidediato clusters derived from a highly reactive ruthenium oxo cluster: synthesis and characterization of $[(\text{PPh}_3)_2\text{N}][\text{MRu}_3(\text{CO})_{12}(\eta^2-\mu_3-\text{NC}(\mu-\text{O})\text{CH}_3)]$, ($\text{M} = \text{Mn}$ or Re) \star

Eric J. Voss¹, Michal Sabat², Duward F. Shriver

Department of Chemistry, Northwestern University, Evanston, IL 60208-3113, USA

Received 17 November 1994; revised 11 July 1995

Abstract

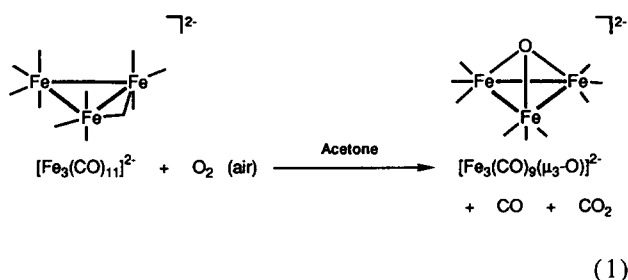
Analogy with the isolable oxo cluster $[\text{Fe}_3(\text{CO})_9(\mu_3-\text{O})]^{2-}$, which is structurally interesting and synthetically useful, prompted the present attempt to synthesize its ruthenium analog. Although the high reactivity of $[\text{Ru}_3(\text{CO})_9(\mu_3-\text{O})]^{2-}$ (**I**) prevented its isolation, the reaction of this species with $[\text{M}(\text{CO})_3(\text{NCCH}_3)]^+$, where $\text{M} = \text{Mn}$ or Re , yields $[\text{PPN}][\text{MRu}_3(\text{CO})_{12}(\eta^2-\mu_3-\text{NC}(\mu-\text{O})\text{CH}_3)]^-$. The high nucleophilicity of the oxo ligand in $[\text{Ru}_3(\text{CO})_9(\mu_3-\text{O})]^{2-}$ (**I**) appears to be responsible for the conversion of acetonitrile to an acetamidediato ligand and for the instability of **I**. The crystal structure of $[\text{PPN}][\text{MnRu}_3(\text{CO})_{12}(\eta^2-\mu_3-\text{NC}(\mu-\text{O})\text{CH}_3)]^-$ reveals a hinged butterfly array of metal atoms in which the acetamidediato ligand bridges the two wings with $\mu_3-\text{N}$ bonding to an Mn and two Ru atoms, and $\mu-\text{O}$ bonding to an Ru atom.

Keywords: Crystal structures; Ruthenium complexes; Manganese complexes; Rhenium complexes; Carbonyl complexes; Acetamidediato complexes; Cluster complexes

1. Introduction

The cluster building chemistry of $[\text{Fe}_3(\text{CO})_9(\mu_3-\text{O})]^{2-}$ investigated in our research group prompted exploration of the preparation and reactivity of the analogous ruthenium cluster. The initial goal was to synthesize the ruthenium oxo cluster $[\text{Ru}_3(\text{CO})_9(\mu_3-\text{O})]^{2-}$, the analog of $[\text{Fe}_3(\text{CO})_9(\mu_3-\text{O})]^{2-}$, and then to utilize this cluster in the synthesis of higher nuclearity mixed-metal oxo clusters.

The chemistry of the anions $[\text{Fe}_3(\text{CO})_{11}]^{2-}$ and $[\text{Ru}_3(\text{CO})_{11}]^{2-}$ has been the subject of much study in our research group and others [1–10]. For example, both $[\text{Fe}_3(\text{CO})_{11}]^{2-}$ and $[\text{Ru}_3(\text{CO})_{11}]^{2-}$ have been used to synthesize the ketylenylidene clusters $[\text{M}_3(\text{CO})_9(\mu_3-\text{CCO})]^{2-}$ ($\text{M} = \text{Fe}$ or Ru) [4,11]. The cluster $[\text{Fe}_3(\text{CO})_{11}]^{2-}$ is also the precursor to $[\text{Fe}_3(\text{CO})_9(\mu_3-\text{O})]^{2-}$ (Eq. (1)), the oxo source for higher nuclearity oxo clusters.



The similarity of the reactivity of $[\text{Ru}_3(\text{CO})_{11}]^{2-}$ to $[\text{Fe}_3(\text{CO})_{11}]^{2-}$ makes the former a likely candidate for the synthesis of an analogous ruthenium oxo cluster; however there are no reports of this compound. The ruthenium oxo cluster $[\text{Ru}_3(\text{CO})_9(\mu_3-\text{O})]^{2-}$ (**I**) was not isolated in the present research but circumstantial evidence is presented for its existence.

This paper also describes the synthesis and characterization of the mixed-metal acetamidediato clusters $[\text{PPN}][\text{MnRu}_3(\text{CO})_{12}(\eta^2-\mu_3-\text{NC}(\mu-\text{O})\text{CH}_3)]^-$ ($[\text{PPN}]$ (**II**)) and $[\text{PPN}][\text{ReRu}_3(\text{CO})_{12}(\eta^2-\mu_3-\text{NC}(\mu-\text{O})\text{CH}_3)]^-$ ($[\text{PPN}]$ (**III**)), which appear to originate from the reaction of $[\text{Ru}_3(\text{CO})_9(\mu_3-\text{O})]^{2-}$ with the lightly stabilized electrophilic compounds $[\text{M}(\text{CO})_3(\text{NCCH}_3)_3]^+$ ($\text{M} = \text{Mn}$ or Re) [12].

\star Dedicated to Fred Basolo, a splendid colleague and scientist.

¹ Present address: Southern Illinois University, Edwardsville, IL 62026, USA.

² Present address: University of Virginia, Charlottesville, VA 22903, USA.

The highly nucleophilic oxo ligand reacts at the carbon of the metal bound acetonitrile ligand of $[M(CO)_3(NCCH_3)_3]^+$ to transform the acetonitrile ligand to a bridging acetamidediato ($\eta^2-\mu_3-NC(\mu-O)CH_3$) ligand. The acetamidediato ligand name is derived from the organic acetamide molecule, CH_3CONH_2 . The conversion of nitriles to amides in organic chemistry is achieved through acid or base catalyzed hydrolysis, and these conversions also have been observed on metal complexes and clusters. The acetamidediato clusters reported in this paper are the first to contain an acetamidediato ligand that is both N-bound and O-bound to a four-metal cluster framework.

2. Experimental

2.1. General procedures and materials

All manipulations were carried out under an atmosphere of pre-purified dry nitrogen by employing standard Schlenk and syringe techniques [13]. Solids were manipulated in a Vacuum Atmospheres glovebox equipped with a recirculator and Dri-Train system. All solvents were distilled from the appropriate drying agents in an air-free environment prior to use [14]. $[\mu\text{-Nitrido-bis(triphenylphosphorus)}(1+)]$ chloride ($[PPN]Cl$) (Alpha Products) was dried in an oven at 110 °C for 24 h prior to use. N_2O and O_2 gas (Matheson Gas) were used as received. Sodium beads, benzophenone (Ph_2CO), iodobenzene ($PhIO$) and $K[BPh_4]$ (Aldrich Chemicals) were also used as received. The compounds $Ru_3(CO)_{12}$ [15], $[Mn(CO)_3(NCCH_3)_3][PF_6]$ [16] and $[Re(CO)_3(NCCH_3)_3][PF_6]$ [17] were prepared following literature procedures. The compound $[PPN]_2[Ru_3(CO)_{11}]$ was prepared by using a modification of a literature procedure (see below) [4,9,10].

Solution IR samples were loaded into CaF_2 windowed cells with 0.1 mm pathlength, and spectra were recorded on a Matteson Alpha Centauri or Bomem MB-100 Fourier transform infrared spectrometer equipped with a DTGS detector. Elemental analyses were performed by Elbach Analytical Laboratories, Postfach 1315, D-5250 Engelskirchen, Germany.

The liquid secondary ion mass spectra (LSIMS, commonly termed FABMS) were obtained on a VG-70SE double-focusing high-resolution mass spectrometer equipped with a VG 11/250J data system. The samples were dissolved in CH_2Cl_2 , and 3-nitrobenzyl alcohol (*m*-NBA) was employed as the matrix. Cesium iodide was used as the primary Cs^+ ion source. The primary ion beam (1 μA at 30 kV) impinged on the liquid sample surface, and negative ion detection was used to collect all mass spectra. The VG software ISO was used to calculate isotopic distributions of molecular ions.

A conventional R factor, $R = (\sum ||I_o - I_c||) / \sum I_o$ (analogous to a crystallographic R factor, in which I_o is the observed intensity and I_c is the calculated intensity at a given mass number) was calculated to provide a quantitative meas-

ure of the fit between calculated isotopomers of the proposed compound and the observed spectrum. Peaks at least five mass units on either side of the most intense peak in the observed spectrum were used in this calculation. Previous workers [18] have determined that the mass spectral assignments are satisfactory when the values of R are roughly similar to those in acceptable crystal structure determinations. According to this criterion, the mass envelopes are convincingly assigned.

2.2. Synthesis of $[PPN]_2[Ru_3(CO)_{11}]$

Samples of $Ru_3(CO)_{12}$ (2.0 g, 3.1 mmol) and oven dried $[PPN]Cl$ (4.0 g, 7.0 mmol, ~ 2.3 equiv.) were placed into a 300 ml Schlenk flask in air, degassed with dry N_2 three times, and suspended in freshly distilled THF (30 ml). The flask was immediately sealed and the reaction mixture was stirred for 1 h, during which the bright orange solid $Ru_3(CO)_{12}$ dissolved. The solution became dark red-brown, and $[PPN][Ru_3(Cl)(CO)_{11}]$ formed [19]. IR ($\nu(CO)$, THF): 2098 (w), 2059 (s), 2025 (vs), 2010 (vs), 1966 (s, sh), 1961 (vs), 1827 (w), cm^{-1} . The IR spectrum also indicated a small amount of $[PPN][Ru_3(\mu-Cl)(CO)_{10}]$ present, ($\nu(CO)$: 1991 (m) cm^{-1}). A reducing solution (30 ml) prepared by vigorously stirring benzophenone (2.0 g, 11 mmol), sodium (0.6 g, 26 mmol) and THF (60 ml) for 45 min was added dropwise to the dark red-brown chloride adduct. Methanol (2 ml) was added to remove excess sodium benzophenone ketyl, the solution volume was reduced in half under vacuum, and Et_2O (50 ml) was added to precipitate the red-brown solid product. The cluster was isolated by filtration, briefly vacuum dried, dissolved in CH_2Cl_2 (25 ml), filtered, and immediately precipitated with Et_2O (50 ml). The resulting red-brown $[PPN]_2[Ru_3(CO)_{11}]$ was washed with methanol (3×10 ml) followed by Et_2O (3×5 ml). Isolated yield 4.9 g (2.9 mmol, 94%). IR ($\nu(CO)$, CH_3CN): 2030 (w), 1959 (s), 1941 (vs), 1878 (m), 1680 (w) cm^{-1} .

2.3. Reaction of $[PPN]_2[Ru_3(CO)_{11}]$ with air

A sample of $[PPN]_2[Ru_3(CO)_{11}]$ (200 mg, 0.118 mmol) was placed into a 100 ml Schlenk flask, dissolved in acetone (50 ml), and filtered. Air that had been passed through a drying tube containing Drierite[®] ($CaSO_4$) was bubbled through the solution for 30 s, and the flask was sealed. The solution was stirred for 30 min and changed from a golden red-brown color to a light orange color to a green-brown color. IR ($\nu(CO)$, acetone): 2015 (m), 1963 (vs), 1992 (s), 1903 (m, sh) cm^{-1} . The solvent was removed under vacuum and the brown oily solids were dissolved in dichloromethane. IR ($\nu(CO)$, CH_2Cl_2): 2019 (m), 1968 (vs), 1925 (s), 1772 (m) cm^{-1} . Subsequent attempts to crystallize the product using various solvent combinations resulted in brown oily solids. The formation of some $[PPN]_2[Ru_4(CO)_{13}]$ is indicated by peaks at 1942 (s) and 1896

(ms) cm^{-1} in the IR spectrum when the sample was left in solution under N_2 over a prolonged period of time (> 12 h).

2.4. Reaction of $[\text{PPN}]_2[\text{Ru}_3(\text{CO})_{11}]$ with O_2 gas

A sample of $[\text{PPN}]_2[\text{Ru}_3(\text{CO})_{11}]$ (250 mg, 0.148 mmol) was placed into a 320 ml gas bulb equipped with a micro stirbar. The red–brown solid was dissolved in acetone (5 ml) and was freeze–pump–thaw degassed three times. A sample of O_2 gas (3.0 torr, 1.5 mmol, 1.33 equiv.) measured with a mercury manometer on the vacuum line was introduced above the frozen solution of $[\text{PPN}]_2[\text{Ru}_3(\text{CO})_{11}]$. The mixture was warmed to room temperature under O_2 , stirred for 1 h, purged with dry N_2 , transferred to a 30 ml Schlenk flask, and filtered. The IR spectrum of the green–orange solution matched those for other reactions in which attempts were made to form $[\text{PPN}]_2[\text{Ru}_3(\text{CO})_9(\mu_3\text{-O})]$. IR ($\nu(\text{CO})$, acetone): 2015 (m), 2012 (w, sh), 1964 (vs), 1921 (s), 1904 (m, sh), 1888 (w, sh) cm^{-1} . Attempts to isolate a crystalline solid were unsuccessful.

2.5. Reaction of $[\text{PPN}]_2[\text{Ru}_3(\text{CO})_{11}]$ with excess N_2O gas

A sample of $[\text{PPN}]_2[\text{Ru}_3(\text{CO})_{11}]$ (60 mg, 0.036 mmol) was placed into a 100 ml Schlenk flask and dissolved in acetone (15 ml). Nitrous oxide gas (N_2O) was bubbled through the solution for 1 min, the flask was sealed, and the solution was stirred. Over a time period of approximately 30 min the solution changed color from golden red–brown, to pale orange–brown, to light orange, and finally to light orange–yellow. The IR spectrum of the light orange–yellow solution matched those for the reaction of O_2 and $[\text{PPN}]_2[\text{Ru}_3(\text{CO})_{11}]$. IR ($\nu(\text{CO})$, acetone): 2016 (m), 1964 (vs), 1921 (s), 1848 (w, sh) cm^{-1} . Attempts to isolate a crystalline solid again proved unsuccessful.

2.6. Reaction of $[\text{PPN}]_2[\text{Ru}_3(\text{CO})_{11}]$ with excess iodosylbenzene

A sample of $[\text{PPN}]_2[\text{Ru}_3(\text{CO})_{11}]$ (50 mg, 0.030 mmol) in a 30 ml Schlenk flask was dissolved in acetone (3 ml) and this solution was syringed into a 30 ml Schlenk flask containing iodosylbenzene (PhIO, 56 mg, 0.25 mmol, ~8 equiv.). After stirring for 3 h, an IR spectrum was obtained which contained more absorption bands and broader bands than in preparations involving O_2 or N_2O . The conclusion from this experiment is that use of excess iodosylbenzene as an oxygen source was not promising. IR ($\nu(\text{CO})$, acetone): 2018 (vs, br), 2007 (m, sh), 1987 (m, br), 1957 (s, sh), 1941 (vs, br) cm^{-1} . The IR peak at 1941 cm^{-1} may indicate the presence of $[\text{PPN}]_2[\text{Ru}_4(\text{CO})_{13}]$ [10].

2.7. Reaction of $[\text{PPN}]_2[\text{Ru}_3(\text{CO})_{11}]$ with one equivalent iodosylbenzene

A sample of $[\text{PPN}]_2[\text{Ru}_3(\text{CO})_{11}]$ (100 mg, 0.059 mmol) in a 30 ml Schlenk flask was dissolved in acetone (3 ml) and

the resulting solution was syringed into a 30 ml Schlenk flask containing iodosylbenzene (PhIO, 13 mg, 0.059 mmol, 1 equiv.). After stirring for 15 min, the IR spectrum again indicated an excessive number of bands. Even the use of only 1 equiv. of iodosylbenzene resulted in a complex mixture. IR ($\nu(\text{CO})$, acetone): 2017 (w, sh), 2004 (m), 1992 (m, br), 1953 (vs), 1943 (s, sh), 1914 (m), 1895 (w, br) cm^{-1} . The IR peak at 1941 cm^{-1} may indicate the presence of $[\text{PPN}]_2[\text{Ru}_4(\text{CO})_{13}]$ [10].

2.8. Metathesis of $[\text{PPN}]_2[\text{Ru}_3(\text{CO})_9(\mu_3\text{-O})]$ to $\text{K}_2[\text{Ru}_3(\text{CO})_9(\mu_3\text{-O})]$

The solution resulting from reaction of $[\text{PPN}]_2[\text{Ru}_3(\text{CO})_{11}]$ (0.036 mmol) with N_2O (above) was vacuum dried to form a yellow glassy material, an excess of $\text{K}[\text{BPh}_4]$ (100 mg, 0.28 mmol, ~8 equiv.) was added in the drybox, and the solids were dissolved in acetone (10 ml). The solution was stirred for 10 min and Et_2O (60 ml) was added, resulting in precipitation of a large quantity of milky white $[\text{PPN}][\text{BPh}_4]$. The yellow–brown solution was isolated by filtration, and the solvent was removed under vacuum, yielding a yellow oil. This oil was dissolved in THF (8 ml) and the IR spectrum was similar to those for other reactions forming $[\text{PPN}]_2[\text{Ru}_3(\text{CO})_9(\mu_3\text{-O})]$. IR ($\nu(\text{CO})$, THF): 2025 (m), 1976 (vs), 1933 (s), 1915 (w, sh), 1788 (s) cm^{-1} . Similar to other experiments, attempts to isolate a crystalline solid proved unsuccessful.

2.9. Synthesis of $[\text{PPN}][\text{MnRu}_3(\text{CO})_{12}(\eta^2\text{-}\mu_3\text{-NC}(\mu\text{-O})\text{-CH}_3)]$ ($[\text{PPN}](\text{II})$)

A sample of $[\text{PPN}]_2[\text{Ru}_3(\text{CO})_{11}]$ (200 mg, 0.118 mmol) was placed into a 100 ml Schlenk flask, dissolved in acetone (10 ml) and filtered. Air that had been passed through a drying tube containing Drierite[®] (CaSO_4) was bubbled through the solution for 30 s, and the flask was sealed. The solution was stirred for 30 min and changed from a golden red–brown color to a light orange color to a green–brown color. IR ($\nu(\text{CO})$, acetone): 2015 (m), 1963 (vs), 1992 (s), 1903 (m, sh) cm^{-1} . The acetone solution was transferred by syringe to a 30 ml Schlenk flask containing a sample of $[\text{Mn}(\text{CO})_3(\text{NCCH}_3)][\text{PF}_6]$ (50 mg, 0.123 mmol, ~1 equiv.) and the solution immediately turned dark brown. The solution was stirred for 2 h, and the IR spectrum indicated reaction had taken place. IR ($\nu(\text{CO})$, acetone): 2051 (m, sh), 2030 (s), 2019 (s), 2009 (vs), 1991 (vs), 1971 (s), 1927 (vs, br), 1857 (w, br), 1809 (m, br) cm^{-1} . Solvent was removed under vacuum to yield a deep red glassy material, which was further vacuum dried for 1 h. The product was extracted into Et_2O (20 ml), isolated by filtration, and dried under vacuum to a red oil. This oil was dissolved in Et_2O (2 ml), and the solution was layered with pentane (8 ml). The resulting deep red crystals of **II** were washed with pentane (2 × 1 ml) and briefly vacuum dried. Isolated yield 10 mg (0.008 mmol, 6.8%). IR ($\nu(\text{CO})$, Et_2O): 2051 (w),

2007 (vs), 1990 (s), 1968 (s), 1924 (w), 1863 (w, br), 1818 (m, br) cm^{-1} . EDAX indicated the presence of P, Mn and Ru in the crystals. *Anal. Calc.* for $\text{C}_{50}\text{H}_{33}\text{N}_2\text{O}_{13}\text{P}_2\text{MnRu}_3$: C, 46.56; H, 2.58; N, 2.17; Mn, 4.26; Ru, 23.51. Found: C, 47.16; H, 2.45; N, 2.02; Mn, 2.71; Ru, 25.10%. The elemental composition of $[\text{MnRu}_3(\text{CO})_{12}(\eta^2\text{-}\mu_3\text{-NC}(\mu\text{-O})\text{CH}_3)]^-$ was confirmed by analysis of the distribution of the isotopomers in the FABMS spectrum reported below. Exposure to the atmosphere was minimized, but the solid compound appears to be stable in air, at least for a short period of time.

2.10. Synthesis of $[\text{PPN}][\text{ReRu}_3(\text{CO})_{12}(\eta^2\text{-}\mu_3\text{-NC}(\mu\text{-O})\text{CH}_3)]^-$ ($[\text{PPN}](\text{III})$)

A sample of $[\text{PPN}]_2[\text{Ru}_3(\text{CO})_{11}]$ (200 mg, 0.118 mmol) was placed into a 100 ml Schlenk flask, dissolved in acetone (10 ml) and filtered. Dry air that had been passed through a drying tube containing Drierite[®] (CaSO_4) was bubbled through the solution for 30 s, and the flask was sealed. The solution was stirred for 30 min and changed from a golden red–brown color to a light orange color to a green–brown color (IR ($\nu(\text{CO})$, acetone): 2015 (m), 1964 (vs), 1922 (s), 1903 (m, sh) cm^{-1}). The acetone solution was transferred by syringe to a 30 ml Schlenk flask containing a sample of $[\text{Re}(\text{CO})_3(\text{NCCH}_3)][\text{PF}_6]$ (65 mg, 0.120 mmol, ~ 1 equiv.) and the resulting solution was a red–brown color that deepened over time. The solution was stirred for 1 h, at which time the IR spectrum indicated reaction had taken place. IR ($\nu(\text{CO})$, acetone): 2051 (m), 2012 (vs), 2003 (m, sh), 1974 (ms), 1952 (s, br), 1914 (m), 1896 (w, br), 1872 (w, sh), 1818 (m) cm^{-1} . The reaction stirred overnight, and other than an increase in intensity of the band at 1975 cm^{-1} , the band pattern of the IR spectrum remained unchanged. The solvent was removed by vacuum to yield a red glassy material, and was vacuum dried for 1 h. The product was extracted into Et_2O (20 ml), isolated by filtration, vacuum dried to a red oil, dissolved in Et_2O (2 ml) and the solution was layered with pentane (6 ml). The resulting deep red crystals of **III** were washed with pentane (2×1 ml) and briefly vacuum dried. Isolated yield 10 mg (0.007 mmol, 6.0%). IR ($\nu(\text{CO})$, Et_2O): 2052 (w), 2018 (m, sh), 2010 (vs), 2003 (s), 1974 (vs), 1937 (s), 1914 (m), 1896 (w), 1869 (w, sh), 1821 (w), 1796 (ms) cm^{-1} . The IR band pattern is similar to that observed for $[\text{PPN}][\text{MnRu}_3(\text{CO})_{12}(\eta^2\text{-NC}(\mu\text{-O})\text{CH}_3)]$. The elemental composition of $[\text{ReRu}_3(\text{CO})_{12}(\eta^2\text{-}\mu_3\text{-NC}(\mu\text{-O})\text{CH}_3)]^-$ was confirmed by analysis of the distribution of the isotopomers in the FABMS spectrum reported below. Exposure to the atmosphere was minimized, but the solid compound appears to be stable in air, at least for a short period of time.

2.11. X-ray crystal structure determination of $[\text{PPN}][\text{MnRu}_3(\text{CO})_{12}(\eta^2\text{-}\mu_3\text{-NC}(\mu\text{-O})\text{CH}_3)]$ ($[\text{PPN}](\text{II})$)

A red, trigonal plate crystal of $[\text{PPN}](\text{II})$ having approximate dimensions of $0.40 \times 0.50 \times 0.15$ mm was mounted on

a glass fiber using high vacuum grease and was immediately put into the cold N_2 stream. All measurements were made on an Enraf-Nonius CAD-4 diffractometer with graphite monochromated $\text{Mo K}\alpha$ radiation.

Cell constants and an orientation matrix for data collection, obtained from a least-squares refinement using the setting angles of 25 carefully centered reflections in the range $27.1 < 2\theta < 28.8^\circ$ corresponded to a triclinic cell with dimensions $a = 11.494(2)$, $b = 13.546(2)$, $c = 16.619(3)$ Å, $\alpha = 94.81(1)$, $\beta = 106.14(1)$, $\gamma = 94.04(1)^\circ$, and $V = 2465(1)$ Å³. For $Z = 2$ and formula weight = 1289.91, the calculated density is 1.738 g cm^{-3} . Based on packing considerations, a statistical analysis of intensity distribution, and the successful solution and refinement of the structure, the space group was determined to be $P\bar{1}$ (No. 2).

The data were collected at a temperature of $-120 \pm 1^\circ\text{C}$ using the $\omega/2\theta$ scan technique to a maximum 2θ value of 46.0° . Omega scans of several intense reflections, made prior to data collection, had an average width at half-height of 0.26° with a take-off angle of 2.8° . Scans of $(0.85 + 0.35 \tan \theta)^\circ$ were made at speeds ranging from 2.0 to $6.0^\circ/\text{min}$ (in omega). Moving-crystal moving-counter background measurements were made by scanning an additional 25% above and below the scan range. The counter aperture consisted of a variable horizontal slit with a width ranging from 2.0 to 2.5 mm and a vertical slit set to 2.0 mm. The diameter of the incident beam collimator was 0.7 mm and the crystal to detector distance was 21 cm. For intense reflections an attenuator was automatically inserted in front of the detector.

Of the 7257 reflections which were collected, 6853 were unique. The intensities of four representative reflections were measured after every 180 min of X-ray exposure time and these remained constant throughout data collection, so no decay correction was applied. The linear absorption coefficient for $\text{Mo K}\alpha$ is 12.5 cm^{-1} . An empirical absorption correction was applied using DIFABS which resulted in transmission factors ranging from 0.89 to 1.10 [20]. The data were corrected for Lorentz and polarization effects.

The structure was solved by direct methods using SHELXS-86 [21]. Three ruthenium atoms and one manganese atom were located on the Patterson map and the other non-hydrogen atoms were found by difference Fourier techniques. The full-matrix least-squares refinement included anisotropic thermal parameters on all non-hydrogen atoms of the cluster and the $[\text{PPN}]^+$ molecule. Hydrogen atoms for all the molecules were introduced at idealized positions and included in structure factor calculations but were not refined. The final cycle of full-matrix least-squares refinement³ was based on 5841 observed reflections ($I > 3.00\sigma(I)$) and 640 variable parameters and converged (largest parameter shift

³ Least-squares: function minimized: $\sum w(|F_o| - |F_c|)^2$ where $w = 4F_o^2 / \sigma^2(F_o^2)$ and $\sigma^2(F_o^2) = [S^2(C + R^2B) + (pF_o^2)^2] / L_p^2$; S = scan rate; C = total integrated peak count; R = ratio of scan time to background counting time; B = total background count; L_p = Lorentz–polarization factor; $p = p$ factor.

was 0.01 times its esd) with unweighted and weighted agreement factors of $R = (\sum ||F_o| - |F_c||) / \sum |F_o| = 0.029$ and $R_w = [(\sum w(|F_o| - |F_c|)^2) / \sum w F_o^2]^{1/2} = 0.043$.

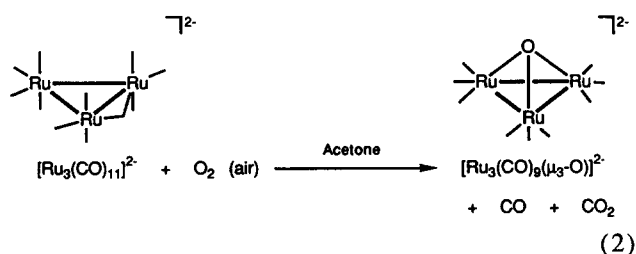
The standard deviation of an observation of unit weight⁴ was 1.40. The weighting scheme was based on counting statistics and included a factor ($p=0.05$) to downweight the intense reflections. Plots of $\sum w(|F_o| - |F_c|)^2$ versus $|F_o|$, reflection order in data collection, $\sin \theta/\lambda$, and various classes of indices showed no unusual trends. The maximum and minimum peaks on the final difference Fourier map corresponded to 1.40 and $-0.50 \text{ e } \text{Å}^{-3}$, respectively.

Neutral atom scattering factors were taken from Cromer and Waber [22]. Anomalous dispersion effects were included in F_{calc} ; the values for $\Delta f'$ and $\Delta f''$ were those of Refs. [23,24]. All calculations were performed using the TEXSAN 4.0 crystallographic software package of Molecular Structure Corporation [25] on a Micro VAX 3600 computer. A summary of the crystallographic data is shown in Table 1.

3. Results and discussion

3.1. Attempted isolation of the ruthenium oxo cluster $[\text{Ru}_3(\text{CO})_9(\mu_3\text{-O})]^{2-}$

The cluster $[\text{PPN}]_2[\text{Ru}_3(\text{CO})_{11}]$ in acetone solution was treated with dry air in an attempt to synthesize $[\text{PPN}]_2[\text{Ru}_3(\text{CO})_9(\mu_3\text{-O})]$, Eq. (2).



The band pattern in the IR spectrum of this ruthenium cluster solution ($\nu(\text{CO})$ 2015 (m), 1964 (vs), 1922 (s), 1905 (m) cm^{-1}) is similar to that of the iron oxo cluster $[\text{Fe}_3(\text{CO})_9(\mu_3\text{-O})]^{2-}$, Fig. 1 [26]. However, only an orange-brown oil could be isolated from the reaction of $[\text{Ru}_3(\text{CO})_{11}]^{2-}$ with air, indicating a mixture. The FABMS spectrum of the oil also is consistent with a mixture of products.

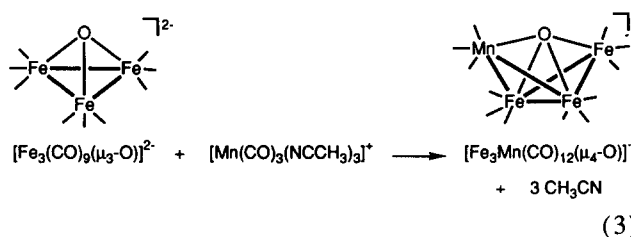
The use of various oxo transfer reagents [27], such as nitrous oxide gas (N_2O), iodosylbenzene (PhIO), and oxygen gas (O_2) with $[\text{Ru}_3(\text{CO})_{11}]^{2-}$ yielded similar mixtures, although the best results were obtained using air as the oxo source. Low temperature reactions also yielded mixtures.

⁴ Standard deviation of an observation of unit weight: $[\sum w(|F_o| - |F_c|)^2 / (N_o - N_v)]^{1/2}$ where N_o = number of observations and N_v = number of variables.

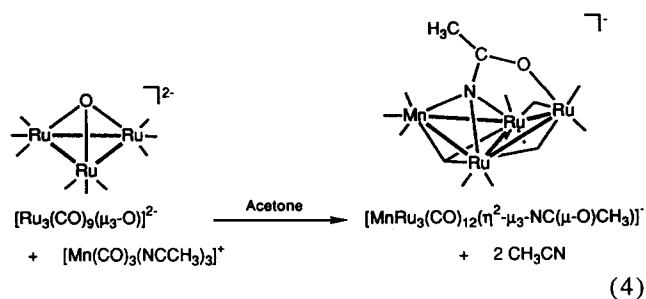
Since a pure oxo cluster was not isolated, the reactions of the oil were investigated, with the thought that an oxo cluster component might exhibit distinctive reactivity.

3.2. Synthesis and characterization of the mixed-metal acetamidediato clusters $[\text{MRu}_3(\text{CO})_{12}(\eta^2\text{-}\mu_3\text{-NC}(\mu\text{-O})\text{CH}_3)]^-$ ($M = \text{Mn}$ or Re)

The iron oxo cluster $[\text{Fe}_3(\text{CO})_9(\mu_3\text{-O})]^{2-}$ reacts with 1 equiv. of $[\text{Mn}(\text{CO})_3(\text{NCCH}_3)_3]^+$ to form the butterfly oxo cluster $[\text{Fe}_3\text{Mn}(\text{CO})_{12}(\mu_4\text{-O})]^-$, Eq. (3) [28]. The monoanionic mixed-metal oxo product exhibited different solubility from the dianionic precursor, and this solubility difference allowed separation of the butterfly cluster from other products of the reaction. This strategy was employed to separate a monoanionic product from the reaction of $[\text{Mn}(\text{CO})_3(\text{NCCH}_3)_3]^+$ with the mixture containing $[\text{Ru}_3(\text{CO})_9(\mu_3\text{-O})]^{2-}$.



An acetone solution of the reaction mixture containing the ruthenium oxo cluster was combined with 1 equiv. of $[\text{Mn}(\text{CO})_3(\text{NCCH}_3)_3][\text{PF}_6]$ [16], in an attempt to mimic Eq. (3). Solvent was removed under vacuum and the resulting dark brown oil was extracted with diethyl ether to give a product (6.6% yield based on $[\text{PPN}]_2[\text{Ru}_3(\text{CO})_{11}]$) with an IR spectrum similar to those for the butterfly clusters $[\text{Fe}_3\text{Mn}(\text{CO})_{12}(\mu_4\text{-O})]^-$ and $[\text{MnRu}_3(\text{CO})_{13}(\mu_4\text{-C})]^-$, Table 2 [28,29]. The monoanionic butterfly cluster resulting from the reaction of $[\text{Ru}_3(\text{CO})_9(\mu_3\text{-O})]^{2-}$ with $[\text{Mn}(\text{CO})_3(\text{NCCH}_3)_3]^+$ is not the expected $[\text{MnRu}_3(\text{CO})_{12}(\mu_4\text{-O})]^-$, but instead is the acetamidediato cluster $[\text{MnRu}_3(\text{CO})_{12}(\eta^2\text{-}\mu_3\text{-NC}(\mu\text{-O})\text{CH}_3)]^-$ (II), Eq. (4).



A negative ion liquid secondary ion (FABMS) mass spectrum of $[\text{PPN}](\text{II})$ was collected, Fig. 2. This compound gave a molecular ion cluster $[M]^-$ at m/z 753, corresponding to $[\text{MnRu}_3(\text{CO})_{12}(\eta^2\text{-}\mu_3\text{-NC}(\mu\text{-O})\text{CH}_3)]^-$, the highest mass ion as well as the most abundant. The fragmentation

Table 1
Summary of the crystallographic data for [PPN][MnRu₃(CO)₁₂(η²-μ₃-NC(μ-O)CH₃)]

<i>Crystal data</i>	
Empirical formula	MnRu ₃ C ₅₀ H ₃₃ N ₂ O ₁₃ P ₂
Formula weight	1289.91
Crystal color, habit	red, trigonal plate
Crystal dimensions (mm)	0.40 × 0.50 × 0.15
Crystal system	triclinic
No. reflections used for unit cell determination (2θ range)	25 (27.1–28.8°)
Omega scan peak width at half-height	0.26
<i>Lattice parameters</i>	
<i>a</i> (Å)	11.494(2)
<i>b</i> (Å)	13.546(2)
<i>c</i> (Å)	16.619(3)
α (°)	94.81(1)
β (°)	106.14(1)
γ (°)	94.04(1)
<i>V</i> (Å ³)	2465(1)
Space group	<i>P</i> $\bar{1}$ (No. 2)
Z value	2
ρ _{calc} (g cm ⁻³)	1.738
<i>F</i> (000)	1276
μ(Mo Kα) (cm ⁻¹)	12.53
<i>Intensity measurements</i>	
Diffractometer	Enraf-Nonius CAD-4
Radiation, λ (Å)	Mo Kα, 0.71069, graphite-monochromated
Temperature (°C)	-120
Attenuator	Zr foil (factor = 20.7)
Take-off angle (°)	2.8
Detector aperture (mm)	2.0–2.5 horizontal, 2.0 vertical
Crystal to detector distance (cm)	21
Scan type	ω/2θ
Scan rate (° min ⁻¹)	2.0–6.0 (in ω)
Scan width (°)	(0.85 + 0.35 tan θ)
2θ Range (°)	4.0–46.0
No. reflections measured	
Total data	7257
Unique data	6853 (<i>R</i> _{int} = 0.015)
Corrections	Lorentz-polarization absorption (transmission factors; 0.89–1.00)
<i>Structure solution and refinement</i>	
Structure solution	direct methods
Refinement	full-matrix least-squares
Function minimized	Σw(<i>F</i> _o - <i>F</i> _c) ²
Least-squares weights	4 <i>F</i> _o ² /σ ² (<i>F</i> _o ²)
<i>p</i> Factor	0.05
Anomalous dispersion	all non-hydrogen atoms
No. observations, <i>I</i> > 3σ(<i>I</i>)	5841
No. variables	640
Reflection/parameter ratio	9.13
<i>Residuals</i>	
<i>R</i> (<i>F</i>) ^a	0.029
<i>R</i> _w (<i>F</i>) ^b	0.043
Goodness of fit indicator	1.40
Maximum shift/error in final cycle	0.01
Maximum peak in final difference map (e Å ⁻³)	1.40
Minimum peak in final difference map (e Å ⁻³)	-0.50

$$^a R(F) = \sum |F_o| - |F_c| / \sum |F_o|$$

$$^b R_w(F) = [(\sum w(|F_o| - |F_c|)^2 / \sum w F_o^2)]^{1/2}$$

pattern in the spectrum of **II** is typical of those observed for carbonyl compounds [30]. Loss of a carbonyl ligand is indicated by a change of 28 in *m/z*, and the spectrum has abundant

ions characteristic of ligand loss. The presence of the acetamidediato ligand presents fragmentation possibilities beyond that of simple carbonyl loss. The fragmentation pattern for

Table 2

IR CO stretching frequencies of the butterfly clusters $[\text{MnRu}_3(\text{CO})_{12}(\eta^2\text{-}\mu_3\text{-NC}(\mu\text{-O})\text{CH}_3)]^-$, $[\text{Fe}_3\text{Mn}(\text{CO})_{12}(\mu_4\text{-O})]^-$ [28] and $[\text{MnRu}_3(\text{CO})_{13}(\mu_4\text{-C})]^-$ [29]

Cluster	Solvent	$\nu(\text{CO})$ (cm^{-1})
$[\text{MnRu}_3(\text{CO})_{12}(\eta^2\text{-}\mu_3\text{-NC}(\mu\text{-O})\text{CH}_3)]^-$	Et_2O	2051 vw, 2007 vs, 1990 s, 1968 s, 1924 w, 1863 w, 1818 m
$[\text{Fe}_3\text{Mn}(\text{CO})_{12}(\mu_4\text{-O})]^-$	CH_2Cl_2	2055 vw, 2005 s, 1986 vs, 1961 w, 1943 w, 1918 vw
$[\text{MnRu}_3(\text{CO})_{13}(\mu_4\text{-C})]^-$	Et_2O	2068 vw, 2023 vs, 1998 m, 1988 m, 1964 w, 1945 w, 1909 vw, 1862 w

vs = very strong; s = strong; ms = medium strong; m = medium; w = weak; vw = very weak; sh = shoulder.

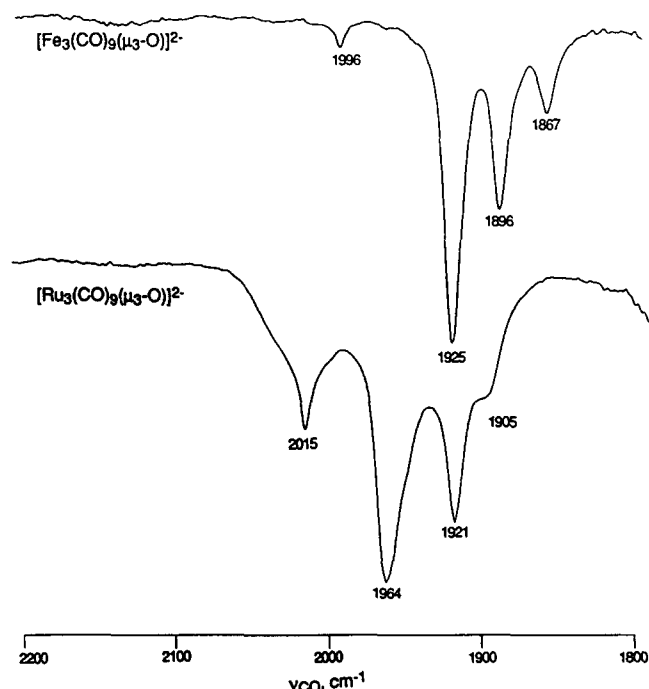


Fig. 1. IR spectra in the carbonyl region of the cluster $[\text{Fe}_3(\text{CO})_9(\mu_3\text{-O})]^{2-}$ and the reaction mixture containing $[\text{Ru}_3(\text{CO})_9(\mu_3\text{-O})]^{2-}$. Spectra were recorded in acetone solution.

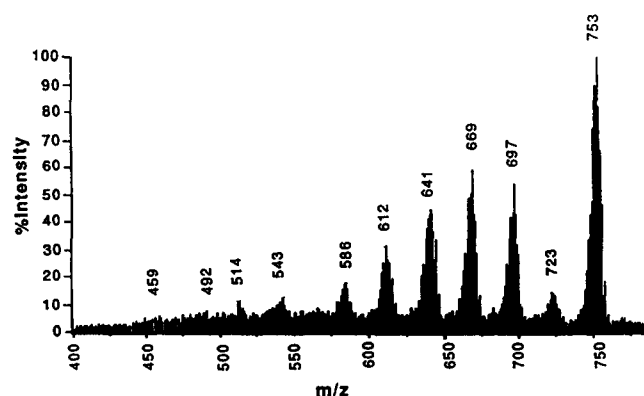


Fig. 2. Negative ion FAB mass spectrum of $[\text{MnRu}_3(\text{CO})_{12}(\eta^2\text{-}\mu_3\text{-NC}(\mu\text{-O})\text{CH}_3)]^-$ in *m*-NBA. Major peaks are labeled with the observed m/z value.

this compound indicates loss of six consecutive carbonyl ligands (theoretical m/z 725, 697, 669, 641, 613, 585), as shown by the ions of high abundance. Lower m/z ions are in low abundance, but there is evidence of loss of the methyl group (m/z 570) and the C(O) from the bridging acetami-

diato ligand (m/z 542), followed by loss of at least two more carbonyl ligands (theoretical m/z 514, 486).

Below these peaks the noise level is too high compared to the peak intensity and reasonable assignments are not possible. Apparently the μ_3 -nitrogen is tightly bound to the cluster framework, as there is no indication of loss of a 14 m/z fragment after loss of the $\text{C}(\text{O})\text{CH}_3$.

For the seven isotopes of ruthenium, the two isotopes each of carbon, oxygen and nitrogen, and the one isotope each of manganese and hydrogen, a wide distribution of peaks (or envelope) would be expected for each ionic species. The isotopic distribution of the envelope surrounding the molecular ion at 752 m/z matches the isotopic distribution expected for $[\text{MnRu}_3(\text{CO})_{12}(\eta^2\text{-}\mu_3\text{-NC}(\mu\text{-O})\text{CH}_3)]^-$, Fig. 3. The low value of $R = (\sum |I_o| - |I_c|) / \sum |I_o| = 0.115$ indicates a good agreement between the calculated mass distribution for $[\text{MnRu}_3(\text{CO})_{12}(\eta^2\text{-}\mu_3\text{-NC}(\mu\text{-O})\text{CH}_3)]^-$ and the observed spectrum. Thus, the mass spectral data are consistent with the X-ray crystal structure of the cluster as [PPN]- $[\text{MnRu}_3(\text{CO})_{12}(\eta^2\text{-}\mu_3\text{-NC}(\mu\text{-O})\text{CH}_3)]^-$ reported below.

An analogous reaction of an acetone solution of the reaction mixture containing the presumed ruthenium oxo cluster $[\text{PPN}]_2[\text{Ru}_3(\text{CO})_9(\mu_3\text{-O})]$ with 1 equiv. of $[\text{Re}(\text{CO})_3\text{-}(\text{NCCH}_3)_3][\text{PF}_6]$ [17], resulted in a butterfly cluster assumed to be $[\text{PPN}][\text{ReRu}_3(\text{CO})_{12}(\eta^2\text{-}\mu_3\text{-NC}(\mu\text{-O})\text{-CH}_3)]$, [PPN] (III), Eq. (5). The IR spectrum of the Et_2O extract from this reaction correlates well with the IR spectrum of $[\text{MnRu}_3(\text{CO})_{12}(\eta^2\text{-}\mu_3\text{-NC}(\mu\text{-O})\text{CH}_3)]^-$ in Et_2O (Table 3), and an analogous compound $[\text{ReRu}_3(\text{CO})_{12}(\eta^2\text{-}\mu_3\text{-NC}(\mu\text{-O})\text{CH}_3)]^-$ is assumed.

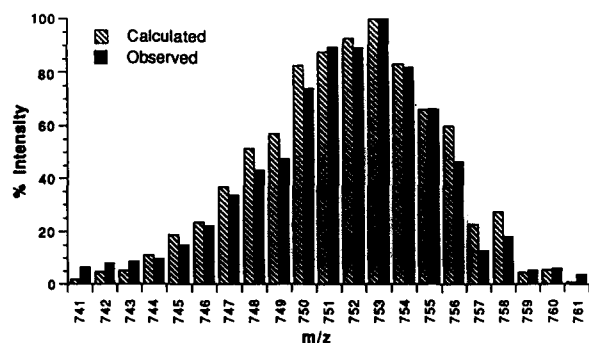


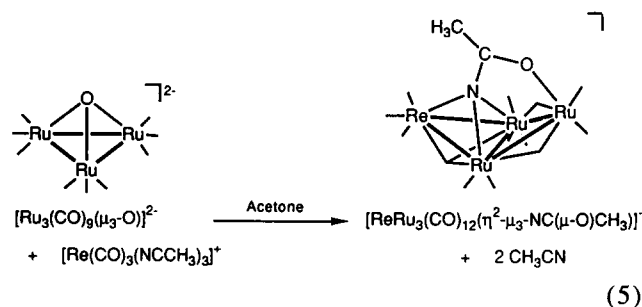
Fig. 3. Observed (solid bar) isotope distribution in the vicinity of 753 m/z in the FAB mass spectrum for Cs^+ bombardment of $[\text{PPN}][\text{MnRu}_3(\text{CO})_{12}(\eta^2\text{-}\mu_3\text{-NC}(\mu\text{-O})\text{CH}_3)]^-$. Dashed bars correspond to the calculated isotopomers of $[\text{MnRu}_3(\text{CO})_{12}(\eta^2\text{-}\mu_3\text{-NC}(\mu\text{-O})\text{CH}_3)]^-$.

Table 3

IR CO stretching frequencies of the butterfly acetamidediato clusters $[\text{MnRu}_3(\text{CO})_{12}(\eta^2\text{-}\mu_3\text{-NC}(\mu\text{-O})\text{CH}_3)]^-$ and $[\text{ReRu}_3(\text{CO})_{12}(\eta^2\text{-}\mu_3\text{-NC}(\mu\text{-O})\text{CH}_3)]^-$

Cluster	Solvent	$\nu(\text{CO})$ (cm^{-1})
$[\text{MnRu}_3(\text{CO})_{12}(\eta^2\text{-}\mu_3\text{-NC}(\mu\text{-O})\text{CH}_3)]^-$	Et_2O	2051 vw, 2007 vs, 1990 s, 1968 s, 1924 w, 1863 w, 1818 m
$[\text{ReRu}_3(\text{CO})_{12}(\eta^2\text{-}\mu_3\text{-NC}(\mu\text{-O})\text{CH}_3)]^-$	Et_2O	2052 w, 2018 sh, 2010 vs, 2003 s, 1974 vs, 1937 s, 1914 m, 1896 m, 1869 w, 1821 w, 1796 ms

vs = very strong; s = strong; ms = medium strong; m = medium; w = weak; vw = very weak; sh = shoulder.



The extra bands in this IR spectrum may be due to other species present in the ether extract. The cluster $[\text{ReRu}_3(\text{CO})_{12}(\eta^2\text{-}\mu_3\text{-NC}(\mu\text{-O})\text{CH}_3)]^-$ was isolated in low yield ($\sim 6\%$) as a red crystalline solid. This chemistry is in contrast to that of the iron oxo cluster $[\text{Fe}_3(\text{CO})_9(\mu_3\text{-O})]^{2-}$ which does not react with $[\text{Re}(\text{CO})_3(\text{NCCH}_3)_3]^+$ [31].

A negative ion liquid secondary ion (FABMS) mass spectrum of $[\text{PPN}][\text{ReRu}_3(\text{CO})_{12}(\eta^2\text{-}\mu_3\text{-NC}(\mu\text{-O})\text{CH}_3)]$ was collected, Fig. 4. This compound gave a molecular ion cluster $[\text{M}]^-$ at m/z 883 corresponding to $[\text{ReRu}_3(\text{CO})_{12}(\eta^2\text{-}\mu_3\text{-NC}(\mu\text{-O})\text{CH}_3)]^-$, the highest mass ion as well as the most abundant.

The fragmentation pattern for compound **III** shows high abundance ions in the high m/z region (loss of carbonyl ligands), low abundance ions in the mid m/z region (fragmentation of the acetamidediato ligand with loss of carbonyl ligands), and then high abundance ions again in the low m/z region (loss of carbonyl ligands). The observed mass spectrum is within experimental error (± 1) of the calculated values that follow. The four consecutive carbonyl ligands (m/z 855, 827, 799, 771) lost are all high abundance ions. In a flat area of the spectrum, the fragmentation of the acetamidediato ligand appears to occur in two ways: loss of a methyl group (m/z 756) with loss of two carbonyl ligands (m/z 728, 700) and simple loss of two carbonyl ligands (m/z 743, 715) followed by loss of a methyl group (m/z 700). Next there appears to be loss of O (m/z 684) and C (m/z 672) from the acetamidediato ligand. Abundant ions again indicate loss of six more carbonyl ligands (m/z 644, 616, 588, 560, 532, 504). Below 500 m/z the noise level is too high compared to the peak intensity to make any reasonable assignments. Apparently the μ_3 -nitrogen is tightly bound to the cluster framework, although there is some evidence of a very small amount of the ion that has lost N of the acetamidediato ligand as well (m/z 658).

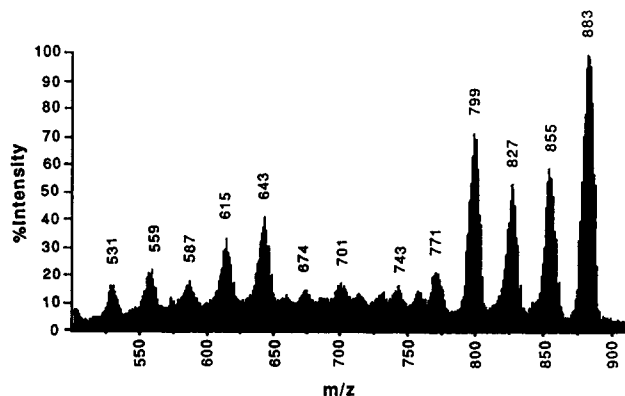


Fig. 4. Negative ion FAB mass spectrum of $[\text{PPN}][\text{ReRu}_3(\text{CO})_{12}(\eta^2\text{-}\mu_3\text{-NC}(\mu\text{-O})\text{CH}_3)]^-$ in m -NBA. Major peaks are labeled with the observed m/z value.

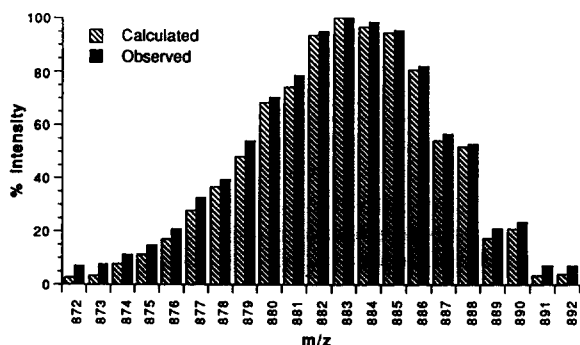


Fig. 5. Observed (solid bar) isotope distribution in the vicinity of 883 m/z in the FAB mass spectrum for Cs^+ bombardment of $[\text{PPN}][\text{ReRu}_3(\text{CO})_{12}(\eta^2\text{-}\mu_3\text{-NC}(\mu\text{-O})\text{CH}_3)]^-$. Dashed bars correspond to the calculated isotopomers of $[\text{ReRu}_3(\text{CO})_{12}(\eta^2\text{-}\mu_3\text{-NC}(\mu\text{-O})\text{CH}_3)]^-$.

For the seven isotopes of ruthenium, the two isotopes each of rhenium, carbon, oxygen and nitrogen, and the one isotope of hydrogen, a wide distribution of peaks (or envelope) would be expected for each ionic species. The isotopic distribution of the envelope surrounding the molecular ion at 883 m/z matches the isotopic distribution expected for $[\text{ReRu}_3(\text{CO})_{12}(\eta^2\text{-}\mu_3\text{-NC}(\mu\text{-O})\text{CH}_3)]^-$, Fig. 5. The low value of $R = (\sum \|I_o\| - |I_c|) / \sum |I_o| = 0.063$ indicates a very good agreement between the calculated mass distribution for $[\text{ReRu}_3(\text{CO})_{12}(\eta^2\text{-}\mu_3\text{-NC}(\mu\text{-O})\text{CH}_3)]^-$ and the observed mass spectrum. Thus, the mass spectral data are consistent with the assignment of the cluster as $[\text{PPN}][\text{ReRu}_3(\text{CO})_{12}(\eta^2\text{-}\mu_3\text{-NC}(\mu\text{-O})\text{CH}_3)]^-$ based on the IR data.

3.3. Structure of $[\text{MnRu}_3(\text{CO})_{12}(\eta^2\text{-}\mu_3\text{-NC}(\mu\text{-O})\text{CH}_3)]^-$

The ORTEP [32] drawing of the structure of $[\text{MnRu}_3(\text{CO})_{12}(\eta^2\text{-}\mu_3\text{-NC}(\mu\text{-O})\text{CH}_3)]^-$ is shown in Fig. 6. Details of the structure including positional parameters, bond distances and bond angles are summarized in Tables 4–6.

The cluster $[\text{MnRu}_3(\text{CO})_{12}(\eta^2\text{-}\mu_3\text{-NC}(\mu\text{-O})\text{CH}_3)]^-$ has a four-metal butterfly geometry consisting of two metal triangles sharing an edge. The manganese metal atom occupies a wingtip position in the butterfly, two ruthenium metals (Ru1 and Ru2) occupy hinge sites, and the third ruthenium (Ru3) is on the other wingtip metal site. Nine of the twelve carbonyl ligands in this cluster are terminal, three on the manganese atom and two on each ruthenium atom. Two μ_2 -carbonyl ligands bridge between the wingtip Ru atom and the hinge Ru atoms, and one μ_3 -CO ligand caps the Mn–Ru1–Ru2 face on the exterior of the cluster opposite the acetamidediato ($\eta^2\text{-}\mu_3\text{-NC}(\mu\text{-O})\text{CH}_3$) ligand. The acetamidediato ligand bridges between the wings of the butterfly and is μ_3 -N-bonded to Mn, Ru1 and Ru2, and O-bonded to the wingtip ruthenium atom, Ru3.

The metal–metal bond distances are typical of those observed in ruthenium butterfly and Ru–Mn clusters [33,34]: Ru1–Ru2 = 2.735(1), Ru1–Ru3 = 2.767(1), Ru2–Ru3 = 2.742(1), Ru1–Mn = 2.794(1), Ru2–Mn = 2.697(1) Å. For reference, the metal–metal bond distances in the cluster $[\eta^5\text{-C}_5\text{H}_5(\text{CO})_2\text{MnRu}_2(\text{CO})_6(\mu_3\text{-PC}_6\text{H}_{11})]$ are: Mn1–Ru1 = 2.838(2), Mn1–Ru2 = 2.848(2), Ru1–Ru2 = 2.826(1) Å [34].

The nitrogen of the acetamidediato ligand is bonded to the metal framework, closer to the wingtip manganese atom (Mn–N1 1.918(3) Å) than the hinge ruthenium atoms (Ru1–N1, 2.126(3); Ru2–N1, 2.116(3) Å). The N1–C1 distance of 1.326(5) Å is intermediate between a single and double nitrogen–carbon bond distance; the C1–O1 distance of 1.264(5) Å is between a single and double carbon–oxygen bond. Based on these bond distances, the bridging acetami-

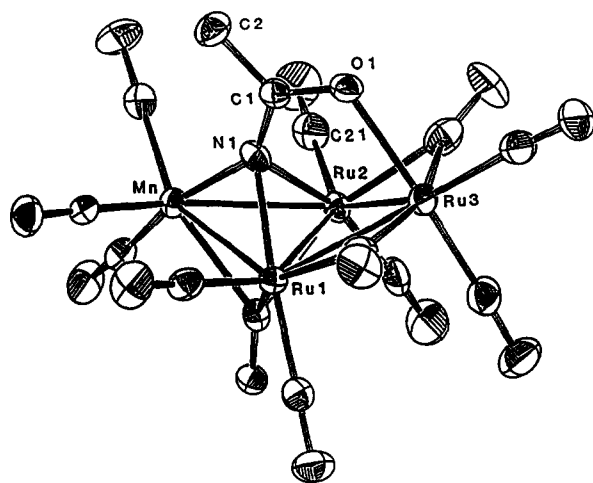


Fig. 6. ORTEP drawing of $[\text{MnRu}_3(\text{CO})_{12}(\eta^2\text{-}\mu_3\text{-NC}(\mu\text{-O})\text{CH}_3)]^-$. Thermal ellipsoids are drawn at a 50% probability level.

Table 4

Positional parameters and their e.s.d.s for [PPN] $[\text{MnRu}_3(\text{CO})_{12}(\eta^2\text{-}\mu_3\text{-NC}(\mu\text{-O})\text{CH}_3)]^-$

Atom	x	y	z	B_{eq}
Ru1	0.05419(3)	0.25070(2)	0.29714(2)	1.59(1)
Ru2	0.17692(3)	0.10656(2)	0.38055(2)	1.74(1)
Ru3	0.08410(3)	0.24648(3)	0.46783(2)	2.08(1)
Mn	0.25237(5)	0.17651(4)	0.25443(4)	1.72(2)
P1	-0.29374(9)	0.33063(7)	-0.05941(6)	1.51(3)
P2	-0.4437(1)	0.33904(7)	-0.23476(6)	1.56(3)
O1	0.2531(2)	0.3381(2)	0.4797(2)	2.2(1)
O11	0.0638(3)	0.4258(2)	0.1938(2)	3.8(1)
O12	-0.2162(3)	0.2035(2)	0.2147(2)	3.3(1)
O21	0.4090(3)	0.0025(3)	0.4102(2)	4.4(2)
O22	0.0309(4)	-0.0920(3)	0.3677(2)	4.5(2)
O31	0.0780(3)	0.3295(3)	0.6429(2)	3.4(1)
O32	-0.1516(3)	0.1199(3)	0.4386(2)	4.3(2)
O41	0.2625(3)	0.3276(2)	0.1397(2)	3.1(1)
O42	0.2455(3)	0.0171(2)	0.1202(2)	3.5(1)
O43	0.5185(3)	0.1754(2)	0.3092(2)	3.5(1)
O51	-0.0412(3)	0.4242(2)	0.3919(2)	3.6(1)
O61	0.2585(3)	0.1079(3)	0.5745(2)	4.1(1)
O71	0.0009(3)	0.0433(2)	0.2017(2)	2.2(1)
N1	0.2431(3)	0.2477(2)	0.3568(2)	1.8(1)
N2	-0.3417(3)	0.3697(2)	-0.1480(2)	1.9(1)
C1	0.2925(4)	0.3221(3)	0.4164(2)	2.0(1)
C2	0.3961(4)	0.3895(3)	0.4099(3)	2.9(2)
C11	0.0585(4)	0.3593(3)	0.2318(3)	2.4(2)
C12	-0.1139(4)	0.2232(3)	0.2462(3)	2.2(2)
C21	0.3221(4)	0.0421(3)	0.3982(3)	2.7(2)
C22	0.0869(4)	-0.0170(4)	0.3762(3)	2.7(2)
C31	0.0826(4)	0.3011(3)	0.5785(3)	2.7(2)
C32	-0.0609(5)	0.1680(3)	0.4518(3)	2.9(2)
C41	0.2594(4)	0.2683(3)	0.1851(3)	2.0(1)
C42	0.2439(4)	0.0780(3)	0.1718(3)	2.2(2)
C43	0.4150(4)	0.1749(3)	0.2881(3)	2.3(2)
C51	0.0061(4)	0.3516(3)	0.3947(3)	2.5(2)
C61	0.2013(4)	0.1356(3)	0.5113(3)	2.8(2)
C71	0.0691(4)	0.1040(3)	0.2495(2)	1.9(1)
C101	-0.1752(3)	0.2506(3)	-0.0577(2)	1.7(1)
C102	-0.1483(4)	0.2217(3)	-0.1323(2)	1.9(1)
C103	-0.0540(4)	0.1623(3)	-0.1310(3)	2.2(1)
C104	0.0112(4)	0.1312(3)	-0.0563(3)	2.7(2)
C105	-0.0135(4)	0.1608(3)	0.0177(3)	2.9(2)
C106	-0.1071(4)	0.2199(3)	0.0179(3)	2.4(2)
C111	-0.2281(3)	0.4362(3)	0.0177(2)	1.6(1)
C112	-0.1610(4)	0.5125(3)	-0.0048(3)	2.1(1)
C113	-0.1079(4)	0.5939(3)	0.0553(3)	2.5(2)
C114	-0.1198(4)	0.5962(3)	0.1359(3)	2.5(2)
C115	-0.1864(4)	0.5198(3)	0.1577(3)	2.4(2)
C116	-0.2409(4)	0.4391(3)	0.0987(3)	2.1(1)
C121	-0.4116(4)	0.2687(3)	-0.0238(2)	1.9(1)
C122	-0.4038(5)	0.1757(3)	0.0048(3)	3.5(2)
C123	-0.4996(6)	0.1348(4)	0.0319(4)	4.8(2)
C124	-0.6005(5)	0.1846(5)	0.0278(3)	4.8(2)
C125	-0.6084(4)	0.2777(5)	-0.0014(3)	4.1(2)
C126	-0.5126(4)	0.3193(4)	-0.0263(3)	2.9(2)
C201	-0.5306(3)	0.4429(3)	-0.2615(2)	1.7(1)
C202	-0.6168(4)	0.4386(3)	-0.3400(2)	1.9(1)
C203	-0.6797(4)	0.5186(3)	-0.3618(3)	2.2(1)
C204	-0.6573(4)	0.6056(3)	-0.3067(3)	2.1(2)
C205	-0.5717(4)	0.6109(3)	-0.2294(3)	2.1(1)
C206	-0.5073(4)	0.5301(3)	-0.2058(2)	1.9(1)
C211	-0.3743(4)	0.3179(3)	-0.3187(2)	2.0(1)

(continued)

Table 6

Selected intramolecular bond angles (°) for [PPN][MnRu₃(CO)₁₂(η^2 - μ_3 -NC(μ -O)CH₃)]^a

Atom 1	Atom 2	Atom 3	Angle	Atom 1	Atom 2	Atom 3	Angle
Ru2	Ru1	Ru3	59.79(2)	Mn	Ru1	C71	52.0(1)
Ru2	Ru1	Mn	58.38(2)	N1	Ru1	C11	100.5(2)
Ru2	Ru1	N1	49.71(9)	N1	Ru1	C12	167.4(1)
Ru2	Ru1	C11	147.3(1)	N1	Ru1	C51	99.6(1)
Ru2	Ru1	C12	118.1(1)	N1	Ru1	C71	82.8(1)
Ru2	Ru1	C51	106.4(1)	C11	Ru1	C12	90.4(2)
Ru2	Ru1	C71	51.6(1)	C11	Ru1	C51	89.9(2)
Ru3	Ru1	Mn	109.91(2)	C11	Ru1	C71	121.2(2)
Ru3	Ru1	N1	72.39(9)	C12	Ru1	C51	86.6(2)
Ru3	Ru1	C11	131.2(1)	C12	Ru1	C71	86.2(2)
Ru3	Ru1	C12	105.1(1)	C51	Ru1	C71	148.1(2)
Ru3	Ru1	C51	46.7(1)	Ru1	Ru2	Ru3	60.69(2)
Ru3	Ru1	C71	106.0(1)	Ru1	Ru2	Mn	61.91(2)
Mn	Ru1	N1	43.29(8)	Ru1	Ru2	N1	50.0(1)
Mn	Ru1	C11	91.4(1)	Ru1	Ru2	C21	143.4(1)
Mn	Ru1	C12	131.0(1)	Ru1	Ru2	C22	116.9(1)
Mn	Ru1	C51	142.3(1)	Ru1	Ru2	C61	110.1(1)
Ru1	Ru2	C71	49.3(1)	C21	Ru2	C61	92.1(2)
Ru3	Ru2	Mn	113.66(2)	C21	Ru2	C71	115.7(2)
Ru3	Ru2	N1	73.07(9)	C22	Ru2	C61	91.5(2)
Ru3	Ru2	C21	137.2(1)	C22	Ru2	C71	84.6(2)
Ru3	Ru2	C22	107.4(1)	C61	Ru2	C71	151.9(2)
Ru3	Ru2	C61	49.9(1)	Ru1	Ru3	Ru2	59.52(2)
Ru3	Ru2	C71	104.9(1)	Ru1	Ru3	O1	83.25(7)
Mn	Ru2	N1	44.99(8)	Ru1	Ru3	C31	154.6(1)
Mn	Ru2	C21	82.4(1)	Ru1	Ru3	C32	93.8(1)
Mn	Ru2	C22	126.5(1)	Ru1	Ru3	C51	53.1(1)
Mn	Ru2	C61	141.3(1)	Ru1	Ru3	C61	108.5(1)
Mn	Ru2	C71	53.3(1)	Ru2	Ru3	O1	85.15(7)
N1	Ru2	C21	99.3(2)	Ru2	Ru3	C31	144.7(1)
N1	Ru2	C22	165.5(2)	Ru2	Ru3	C32	93.2(1)
N1	Ru2	C61	99.2(1)	Ru2	Ru3	C51	112.5(1)
N1	Ru2	C71	81.4(1)	Ru2	Ru3	C61	49.4(1)
C21	Ru2	C22	90.0(2)	O1	Ru3	C31	90.6(1)
O1	Ru3	C32	177.1(2)	Ru2	Mn	C42	111.2(1)
O1	Ru3	C51	83.9(1)	Ru2	Mn	C43	104.4(1)
O1	Ru3	C61	84.2(1)	Ru2	Mn	C71	51.5(1)
C31	Ru3	C32	92.1(2)	N1	Mn	C41	105.7(2)
C31	Ru3	C51	101.9(2)	N1	Mn	C42	162.5(2)
C31	Ru3	C61	95.3(2)	N1	Mn	C43	95.1(2)
C32	Ru3	C51	94.5(2)	N1	Mn	C71	84.5(1)
C32	Ru3	C61	96.6(2)	C41	Mn	C42	91.0(2)
C51	Ru3	C61	159.2(2)	C41	Mn	C43	92.8(2)
Ru1	Mn	Ru2	59.72(2)	C41	Mn	C71	118.0(2)
Ru1	Mn	N1	49.5(1)	C42	Mn	C43	89.3(2)
Ru1	Mn	C41	93.3(1)	C42	Mn	C71	83.0(2)
Ru1	Mn	C42	125.8(1)	C43	Mn	C71	148.2(2)
Ru1	Mn	C43	144.3(1)	Ru3	O1	C1	112.3(3)
Ru1	Mn	C71	48.1(1)	Ru1	N1	Ru2	80.3(1)
Ru2	Mn	N1	51.3(1)	Ru1	N1	Mn	87.2(1)
Ru2	Mn	C41	151.6(1)	Ru1	N1	C1	114.9(3)
Ru2	N1	Mn	83.7(1)	Ru1	C51	O51	133.0(4)
Ru2	N1	C1	123.9(3)	Ru3	C51	O51	146.7(4)
Mn	N1	C1	145.8(3)	Ru2	C61	Ru3	80.7(2)
P1	N2	P2	139.2(2)	Ru2	C61	O61	138.4(4)
O1	C1	N1	121.6(4)	Ru3	C61	O61	140.7(4)
O1	C1	C2	118.2(4)	Ru1	C71	Ru2	79.1(1)
N1	C1	C2	120.2(4)	Ru1	C71	Mn	79.9(1)
Ru1	C11	O11	178.3(4)	Ru1	C71	O71	133.5(3)
Ru1	C12	O12	178.0(4)	Ru2	C71	Mn	75.2(1)
Ru2	C21	O21	178.6(4)	Ru2	C71	O71	133.4(3)

(continued)

Table 6 (continued)

Atom 1	Atom 2	Atom 3	Angle	Atom 1	Atom 2	Atom 3	Angle
Ru2	C22	O22	175.3(4)	Mn	C71	O71	133.1(3)
Ru3	C31	O31	176.9(4)	C1	C2	H1	114.70
Ru3	C32	O32	177.3(4)	C1	C2	H2	114.05
Mn	C41	O41	179.2(4)	C1	C2	H3	118.04
Mn	C42	O42	176.1(4)	H1	C2	H2	108.99
Mn	C43	O43	178.9(4)	H1	C2	H3	107.35
Ru1	C51	Ru3	80.3(2)	H2	C2	H3	91.15

* E.s.d.s in the least significant figure are given in parentheses.

μ_3 -N-bound to the triangle consisting of the two ruthenium hinge atoms and the wingtip manganese atom, and is also O-bound to the wingtip ruthenium atom. The clusters $[\text{HOs}_4(\text{CO})_{12}(\mu_3\text{-N}(\text{CO})\text{CH}_3)\text{MPPh}_3]$ (M = Au or Cu) are formed by reaction of $[\text{HOs}_4(\text{CO})_{12}(\mu_3\text{-N}(\text{CO})\text{-CH}_3)]^-$ with $[\text{M}(\text{PPh}_3)]^+$ in the presence of $\text{Ti}[\text{PF}_6]$. To our knowledge, the clusters presented in this paper provide the only known examples of an N- and O-bonded acetamidate ligand bridging four metals.

Bridging acetamidate ligands have also been observed in the tetrabridged dirhodium compounds $[\text{Rh}_2(\text{CH}_3\text{CONH})_4(\text{MPh}_3)_2]$ (M = P, As, or Sb) [46] and $[\text{Rh}_2(\text{CH}_3\text{CO}_2)_n(\text{CH}_3\text{CONH})_{4-n}]$ ($n = 0, 1, 2, 3$) [47]. These complexes are made from the analogous acetate bridged compounds, and the acetamidate ligands in them are N-bound to one metal center, and O-bound to the other. A similar bridging acetamidate ligand was also proposed for the triangular cluster $[\text{Os}_3(\text{CO})_{10}(\mu\text{-H})(\text{NHCOR})]$ (R = H, Me, Ph, Et, or Pr) [48]. This cluster was synthesized by reaction of the lightly stabilized osmium cluster $[\text{Os}_3(\text{CO})_{10}(\text{NCCH}_3)_2]$ with RCONH_2 .

The reaction of the acetonitrile ligand on $[\text{Mn}(\text{CO})_3(\text{NCCH}_3)_3]^+$ with the ruthenium oxo cluster $[\text{Ru}_3(\text{CO})_9(\mu_3\text{-O})]^{2-}$ to form $[\text{MnRu}_3(\text{CO})_{12}(\eta^2\text{-}\mu_3\text{-NC}(\mu\text{-O})\text{CH}_3)]^-$ (II) is in contrast to the reaction of $[\text{Mn}(\text{CO})_3(\text{NCCH}_3)_3]^+$ with the analogous iron oxo cluster $[\text{Fe}_3(\text{CO})_9(\mu_3\text{-O})]^{2-}$. In that chemistry, the acetonitrile ligands are completely lost and the butterfly oxo compound $[\text{Fe}_3\text{Mn}(\text{CO})_{12}(\mu_4\text{-O})]^-$ is formed. Also, although no reaction was observed between $[\text{Fe}_3(\text{CO})_9(\mu_3\text{-O})]^{2-}$ and $[\text{Re}(\text{CO})_3(\text{NCCH}_3)_3]^+$, the ruthenium oxo cluster does react with $[\text{Re}(\text{CO})_3(\text{NCCH}_3)_3]^+$ to form the acetamidate cluster $[\text{ReRu}_3(\text{CO})_{12}(\eta^2\text{-}\mu_3\text{-NC}(\mu\text{-O})\text{CH}_3)]^-$ (III). Apparently, the oxo ligand in $[\text{Ru}_3(\text{CO})_9(\mu_3\text{-O})]^{2-}$ is much more nucleophilic and thus more reactive than the oxo ligand in $[\text{Fe}_3(\text{CO})_9(\mu_3\text{-O})]^{2-}$. This high reactivity may help to rationalize the difficulty in isolating pure $[\text{Ru}_3(\text{CO})_9(\mu_3\text{-O})]^{2-}$, and the low yields of the acetamidate clusters $[\text{MnRu}_3(\text{CO})_{12}(\eta^2\text{-}\mu_3\text{-NC}(\mu\text{-O})\text{CH}_3)]^-$ (II) and $[\text{ReRu}_3(\text{CO})_{12}(\eta^2\text{-}\mu_3\text{-NC}(\mu\text{-O})\text{CH}_3)]^-$ (III) in these reactions.

4. Conclusions

The interesting chemistry of the iron oxo cluster $[\text{Fe}_3(\text{CO})_9(\mu_3\text{-O})]^{2-}$ prompted research into the prepara-

tion and reactivity of the analogous ruthenium oxo cluster. Unlike the iron analog, $[\text{Ru}_3(\text{CO})_{11}]^{2-}$ reacts with oxygen sources to form a mixture of products, in which $[\text{Ru}_3(\text{CO})_9(\mu_3\text{-O})]^{2-}$ (I) is believed to be one component.

When the mixture containing $[\text{Ru}_3(\text{CO})_9(\mu_3\text{-O})]^{2-}$ is allowed to react with the electrophilic compounds $[\text{M}(\text{CO})_3(\text{NCCH}_3)_3]^+$ (M = Mn or Re), the mixed-metal butterfly clusters $[\text{MnRu}_3(\text{CO})_{12}(\eta^2\text{-}\mu_3\text{-NC}(\mu\text{-O})\text{CH}_3)]^-$ (M = Mn or Re) are formed. Unlike the products from analogous chemistry with the iron oxo cluster which contain a μ_4 -oxo ligand, these clusters contain a bridging acetamidate ligand. Acetamidate ligands have been observed on previously studied clusters, but $[\text{MnRu}_3(\text{CO})_{12}(\eta^2\text{-}\mu_3\text{-NC}(\mu\text{-O})\text{CH}_3)]^-$ and $[\text{ReRu}_3(\text{CO})_{12}(\eta^2\text{-}\mu_3\text{-NC}(\mu\text{-O})\text{-CH}_3)]^-$ are the first examples to contain an acetamidate ligand that is both N-bonded and O-bonded to the cluster framework. The acetamidate ligand functions as a six-electron donor to the butterfly of metal atoms.

The oxo cluster I is apparently much more reactive than the iron analog, $[\text{Fe}_3(\text{CO})_9(\mu_3\text{-O})]^{2-}$ as is evidenced by reaction with the acetonitrile ligand in $[\text{M}(\text{CO})_3(\text{NCCH}_3)_3]^+$ (M = Mn or Re) to produce an acetamidate ligand in the butterfly clusters II and III.

Acknowledgements

We appreciate the support of this research by the Department of Energy, Basic Energy Science Program, Award No. DE-FG02-86ER13640.

References

- [1] D.F. Shriver, D. Lehman and D. Stroppe, *J. Am. Chem. Soc.*, **97** (1975) 1594.
- [2] H.A. Hodali, D.F. Shriver and C.A. Ammlung, *J. Am. Chem. Soc.*, **100** (1978) 5239.
- [3] H.A. Hodali and D.F. Shriver, *Inorg. Synth.*, **20** (1980) 222.
- [4] M.J. Sailor, C.P. Brock and D.F. Shriver, *J. Am. Chem. Soc.*, **109** (1987) 6015.
- [5] W. Hieber, J. Selemir and R. Werner, *Chem. Ber.*, **90** (1957) 278.
- [6] W. Hieber and H. Beutner, *Z. Naturforsch., Teil B*, **17** (1962) 211.
- [7] W. Hieber and D.H. Schubert, *Z. Anorg. Allg. Chem.*, **338** (1965) 37.
- [8] K. Farmery, M. Kilner, R. Greatrex and N.N. Greenwood, *J. Chem. Soc. A*, (1969) 2339.

- [9] C.C. Nagel, J.C. Bricker, D.G. Alway and S.G. Shore, *J. Organomet. Chem.*, 219 (1981) C9.
- [10] A.A. Bhattacharyya, C.C. Nagel and S.G. Shore, *Organometallics*, 2 (1983) 1187.
- [11] J.W. Kolis, E.M. Holt, M.A. Drezdson, K.H. Whitmire and D.F. Shriver, *J. Am. Chem. Soc.*, 104 (1982) 6134.
- [12] E.J. Voss, M. Sabat and D.F. Shriver, *Inorg. Chem.*, 30 (1991) 2705.
- [13] D.F. Shriver and M.A. Drezdson, *Manipulation of Air-Sensitive Compounds*, Wiley, New York, 2nd edn., 1986, p. 326.
- [14] A.J. Gordon and R.A. Ford, *The Chemist's Companion*, Wiley, New York, 1977, p. 537.
- [15] M.I. Bruce, J.G. Matison, R.C. Wallis, J.M. Patrick, B.W. Skelton and A. White, *J. Chem. Soc., Dalton Trans.*, (1983) 2365.
- [16] D. Drew, D.J. Darensbourg and M.Y. Darensbourg, *Inorg. Chem.*, 14 (1975) 1579.
- [17] R.H. Reimann and E. Singleton, *J. Organomet. Chem.*, 59 (1973) C24.
- [18] M.A. Andrews and H.D. Kaesz, *J. Am. Chem. Soc.*, 101 (1979) 7238.
- [19] S. Han, G.L. Geoffroy, B.D. Dombek and A.L. Rheingold, *Inorg. Chem.*, 27 (1988) 4355.
- [20] N. Walker and D. Stuart, *Acta Crystallogr., Sect. A*, 39 (1983) 158.
- [21] G.M. Sheldrick, *SHELXS-86*, a program for crystal structure determination, University of Göttingen, Germany, 1986.
- [22] D.T. Cromer and J.T. Waber, in J.A. Ibers and W.C. Hamilton (eds.), *International Tables for X-ray Crystallography*, Vol. 4, Kynoch, Birmingham, UK, 1974, Table 2.2 A.
- [23] J.A. Ibers and W.C. Hamilton, *Acta Crystallogr.*, 17 (1964) 781.
- [24] D.T. Cromer, in J.A. Ibers and W.C. Hamilton, *International Tables for X-ray Crystallography*, Vol. 4, Kynoch, Birmingham, UK, 1974, Table 2.3.1.
- [25] P.N. Swepston, *TEXSAN*, Version 4.0, the *TEXRAY* structure analysis program package, Molecular Structure Corporation, College Station, TX, 1987.
- [26] A. Ceriotti, L. Resconi, F. Demartin, G. Longoni, M. Manassero and M. Sansoni, *J. Organomet. Chem.*, 249 (1983) C35.
- [27] R.H. Holm, *Chem. Rev.*, 99 (1987) 275.
- [28] C.K. Schauer and D.F. Shriver, *Angew. Chem., Int. Ed. Engl.*, 26 (1987) 255.
- [29] M.P. Jensen, W. Henderson, D.H. Johnston, M. Sabat and D.F. Shriver, *J. Organomet. Chem.*, 394 (1990) 121.
- [30] S. Naylor and M.D. Vargas, *J. Organomet. Chem.*, 386 (1990) 275.
- [31] C.K. Schauer, S. Harris, M. Sabat, E.J. Voss and D.F. Shriver, submitted for publication.
- [32] C.K. Johnson, ORTEP-II, a FORTRAN thermal-ellipsoid plot program, *Rep. ORNL-5138*, Oak Ridge National Laboratory, Oak Ridge, TN, 1976.
- [33] E. Sappa, A. Tiripicchio, A.J. Carty and G.E. Toogood, *Prog. Inorg. Chem.*, 35 (1987) 437.
- [34] J. Schneider, L. Zsolnai and G. Huttner, *Chem. Rev.*, 115 (1982) 989.
- [35] B.F.G. Johnson, J. Lewis, B. Reichert, K.T. Schorpp and G.M. Sheldrick, *J. Chem. Soc., Dalton Trans.*, (1977) 1417.
- [36] J.S. Bradley, G.B. Ansell and E.W. Hill, *J. Am. Chem. Soc.*, 101 (1979) 7417.
- [37] L.H. Staal, L.H. Polm, K. Vrieze, F. Ploeger and C.H. Stam, *Inorg. Chem.*, 20 (1981) 3590.
- [38] J.W. Lauher, *J. Am. Chem. Soc.*, 100 (1978) 5305.
- [39] P.L. Compagnon and M.L. Miocque, *Ann. Chim.*, 5 (1970) 11.
- [40] W. Wenner, *Org. Synth.*, 4 (1963) 760.
- [41] J.E. McIsaac, Jr., R.E. Ball and E.J. Behrman, *J. Org. Chem.*, 36 (1971) 3048.
- [42] K.B. Wiberg, *J. Am. Chem. Soc.*, 75 (1953) 3961.
- [43] K.B. Wiberg, *J. Am. Chem. Soc.*, 77 (1955) 2519.
- [44] D.A. Buckingham, A.M. Sargeson and A. Zanella, *J. Am. Chem. Soc.*, 94 (1972) 8246.
- [45] J. Puga, A. Arce, R.A. Sanchez-Delgado, J. Ascanio, A. Andriollo, D. Braga and F. Grepioni, *J. Chem. Soc., Dalton Trans.*, (1988) 913.
- [46] S.P. Best, P. Chandley, R.J.H. Clark, S. McCarthy, M.B. Hursthouse and P.A. Bates, *J. Chem. Soc., Dalton Trans.*, (1989) 581.
- [47] M.Y. Chavan, T.P. Zhu, X.Q. Lin, M.Q. Ahsan, J.L. Bear and K.M. Kadish, *Inorg. Chem.*, 23 (1984) 4538.
- [48] T.I. Odiaka, *J. Organomet. Chem.*, 284 (1985) 95.